High-expanding regions in primate cortical brain evolution support supramodal cognitive flexibility

Markus H. Sneve[1*], Håkon Grydeland[1], Marcello G. P. Rosa[2,3,4], Tomáš Paus[5,6,7,8], Tristan Chaplin[2,3,4], Kristine Walhovd[1,9], & Anders M. Fjell[1,9]

[1]Center for Lifespan Changes in Brain and Cognition, Department of Psychology, University of Oslo, Oslo, Norway

[2]Department of Physiology, Monash University, Clayton, VIC 3168, Australia

[3]Biomedicine Discovery Institute, Monash University, Clayton, VIC 3168, Australia

[4]Australian Research Council, Centre for Excellence for Integrative Brain Function, Monash University, Clayton, VIC 3168, Australia

[5]Rotman Research Institute, University of Toronto, Toronto, Canada M6A 2E1

[6]Department of Psychiatry, University of Toronto, Toronto, Canada M5S 1A1

[7]Center for Developing Brain, Child Mind Institute, New York, NY 10022, USA

[8]Department of Psychology, University of Toronto, Toronto, Canada M5S 1A1

[9]Department of Radiology and Nuclear Medicine, Oslo University Hospital, Oslo, Norway

Address correspondence to:

Markus Handal Sneve, Dept. of Psychology. Pb. 1094 Blindern, 0317 Oslo, Norway

Phone: +47 22 84 52 16; E-mail: m.h.sneve@psykologi.uio.no

Abstract

Primate cortical evolution has been characterized by massive and disproportionate expansion of a set of specific regions in the neocortex. The associated increase in neocortical neurons comes with a high metabolic cost, thus the functions served by these regions must have conferred significant evolutionary advantage. In the present series of analyses, we show that evolutionary high-expanding cortex – as estimated from patterns of surface growth from several primate species – shares functional connections with different brain networks in a context-dependent manner. Specifically, we demonstrate that high-expanding cortex is characterized by high internetwork functional connectivity; is recruited flexibly over many different cognitive tasks; and changes its functional coupling pattern between rest and a multimodal task-state. The capacity of high-expanding cortex to connect flexibly with various specialized brain networks depending on particular cognitive requirements suggests that its selective growth and sustainment in evolution may have been linked to an involvement in supramodal cognition. In accordance with an evolutionary-developmental view, we find that this observed ability of high-expanding regions – to flexibly modulate functional connections as a function of cognitive state – emerges gradually through childhood, with a prolonged developmental trajectory plateauing in young adulthood.

Keywords

cerebral cortex, functional connectivity, human brain evolution, human development, multi-modal integration

The most striking feature of the human brain when compared with brains of other primates, is its massively expanded cerebral cortex, mainly due to a higher number of cortical neurons (Herculano-Houzel 2012; Buckner and Krienen 2013). The growth of the primate cortex has not been uniform, however, with a set of so-called 'hotspot' regions in lateral temporal, parietal and prefrontal cortex showing disproportionally high expansion (Hill et al. 2010; Chaplin et al. 2013). Well-supported models suggest that this non-uniform growth has followed allometric scaling laws, and that the massive expansion of certain regions in evolution therefore is a predicted consequence of growing a bigger brain (Finlay and Darlington 1995; Toro et al. 2008; Herculano-Houzel 2012; Chaplin et al. 2013; Rilling 2014; Amlien et al. 2016; although see e.g. Smaers et al. 2017). Nevertheless, the metabolic costs associated with sustaining a higher number of neurons are high (Ringo 1991; Herculano-Houzel 2011) and impose limitations on the growth of other, non-neuronal, physical capacities such as body size (Fonseca-Azevedo and Herculano-Houzel 2012). An intriguing question is therefore: what functions do high-expanding regions in primate brain evolution serve, which may have offset these potential natural selection costs?

Expansion 'hotspots' refer to the cortical regions that differ the most between extant primates of different brain sizes (Chaplin et al. 2013) and are considered a useful proxy for the parts of cortex that have undergone the most expansion during evolution (Hill et al. 2010; Buckner and Krienen 2013). As prototypical members of association cortex, these evolutionary high-expanding regions are involved in various tasks and functional systems and have been theorized to serve relational reasoning and integrative higher-order cognition (Krienen et al. 2014; Vendetti and Bunge 2014). In support of these views, measures of general cognitive abilities in human adults have been shown to correlate positively with

cortical surface-area within high-expanding regions (Fjell et al. 2015), associations not found within low-expanding cortex (Vuoksimaa et al. 2016). Furthermore, when compared with brain regions showing less evolutionary expansion, high-expanding cortex shows higher growth of the surface area during human development (Hill et al. 2010; Amlien et al. 2016), and this pattern is more pronounced in individuals with high intelligence (Schnack et al. 2015).

In the current study, we tested the hypothesis that the growth and sustainment of high-expanding cortex has facilitated supramodal cognition (Goldman-Rakic 1988), conceptualized as the integration of information from across the brain in a flexible manner. By taking advantage of recent developments in brain network analysis (Rubinov and Sporns 2010), and applying these to histological data and magnetic resonance imaging (MRI) scans of multiple primate brains, as well as a large sample of humans during different cognitive states and at different stages in development, we were able to directly test the predictions that high-expanding cortex 1) has broad functional connections with different specialized brain networks; 2) is flexibly engaged by a diverse set of cognitive tasks; 3) is more central to communication flow in the brain during states requiring multimodal integration than during low-demand states; 4) increases functional coupling preferentially with regions engaged by the current cognitive demands. Moreover, given the correlation between morphological changes in primate brain evolution and human development, we predict that the functional connectivity patterns associated with supramodal cognition develop gradually, and fully emerge relatively late in postnatal life.

Materials and Methods

Human subjects

RsfMRI-data were collected in 221 healthy young adults (age range 18-38, mean age 23.8; 142 females). Task-fMRI data were collected in 105 of the same participants (age range 18-38, mean age 25.3; 69 females), as well as in 46 children and adolescents (age range 6-17, mean age 12.9; 21 females). The study was approved by the Regional Ethical Committee of South Norway, and participants provided written informed consent. Participants were required to be right-handed, speak Norwegian fluently and have (corrected to) normal hearing and vision. Clinical sequences (T2-FLAIR) were inspected by a neuroradiologist and deemed free of significant injuries or conditions.

Non-human primates

Evolutionary cortical expansion was calculated from the brains of four simian primates: marmoset (*Callithrix jacchus*), capuchin (*Cebus apella*), macaque (*Macaca mulatta*) and human. Details about the calculations have been described in a previous publication (Chaplin et al. 2013). Briefly, surface models of the cerebral cortex of the four species were registered by deforming the models to align a set of landmarks, consisting of well-established homologous cortical regions, using the CARET software package (Van Essen et al. 2001). Expansion was calculated as the change in size of each mesh polygon, and was averaged across the marmoset to capuchin, marmoset to macaque, and macaque to human deformations. All tests involving comparisons with evolutionary expansion were restricted to measures extracted from right-hemispheric nodes. For the "State-dependent coupling analyses" (Fig. 2), and the "Developmental sample analyses" (Fig. 3), cortical nodes were

binned per evolutionary expansion (SFig. 5). We considered the 20% highest-expanding nodes 'hotspot' regions, and this definition revealed three separate clusters commonly discussed in the literature (Hill et al. 2010; Chaplin et al. 2013).

Experimental design

Resting-state fMRI was collected during eyes-closed rest. Participants were instructed to not fall asleep. Given recent reports that eyes-closed resting-state is associated with higher levels of unintentional sleep among participants when compared to eyes-open rest (Tagliazucchi & Laufs, 2014), the current sample only included participants that confirmed compliance and reported that they remained awake throughout the scan. During the fMRI-task, participants sequentially viewed 100 line drawings of objects and immediately produced a motor response indicating whether the object was congruent with a spoken action (either "Can you eat it" or "Can you lift it"; SFig. 3). The task is described in detail elsewhere (Sneve et al. 2015).

MRI acquisition

Imaging was performed at a Siemens Skyra 3T MRI unit with a 24-channel head coil. For the fMRI scans (rest and task), 43 slices (transversal, no gap) were measured using T2* BOLD EPI (TR=2390 ms; TE=30 ms; flip angle=90°; voxel size=3x3x3 mm; FOV=224x224; interleaved acquisition; GRAPPA=2). The rsfMRI run produced 150 volumes and lasted ≈6 min. The task data were collected over 2 runs, each consisting of 131 volumes and lasting ≈5.2 min. Three dummy volumes were collected at the start of each fMRI scan to avoid T1 saturation effects in the analyzed data. A standard double-echo gradient-echo field map was acquired for distortion correction of the EPI images. Anatomical T1-weighted MPRAGE images consisting

of 176 sagittally oriented slices were obtained using a turbo field echo pulse sequence (TR=2300 ms, TE=2.98 ms, flip angle=8°, voxel size=1×1×1 mm, FOV=256×256 mm).

MRI preprocessing

Cortical reconstruction of the T1-weighted scans was performed with Freesurfer 5.3's recon-all routines, and included surface inflation (Fischl et al., 1999a) and registration to a spherical atlas which utilized individual cortical folding patterns to match cortical geometry across subjects (Fischl et al., 1999b). Functional MRI-data were corrected for B0 inhomogeneity, motion and slice timing corrected, and smoothed (5mm FWHM) in native volume space using FSL (http://fsl.fmrib.ox.ac.uk/fsl/fslwiki). Next, FMRIB's ICA-based Xnoiseifier (FIX; Salimi-Khorshidi et al. 2014) was used to auto-classify noise components and remove them from the fMRI data. Such ICA-based procedure for denoising fMRI data has been shown to effectively reduce motion-induced variability, outperforming methods based on removing motion spikes in the dataset (Pruim et al., 2015). Importantly, different classifiers were used for rsfMRI and task-fMRI data. Classifiers were trained on scanner-specific datasets in which rsfMRI/task-fMRI data from 16 participants had been manually classified into signal and noise components (fMRI acquisition parameters identical to the current study). Motion confounds (24 parameters) were regressed out of the fMRI data as a part of the FIX routines. Freesurfer-defined individually estimated anatomical masks of cerebral white matter (WM) and cerebrospinal fluid / lateral ventricles (CSF) were resampled to each individual's functional space. Following FIX, average time series were extracted from functional WM- and CSF-voxels and were regressed out of the FIX-cleaned 4D volume. Following recent recommendations (Hallquist et al. 2013) we band-pass filtered the rsfMRI data (.009-.08Hz)

after regression of confound variables. Task-fMRI data were detrended and highpass filtered with a .01Hz cutoff.

Network analysis of rsfMRI data

A custom cortical parcellation was created in Freesurfer's average surface space (fsaverage), using a modified N-cut algorithm (Craddock et al. 2012), consisting of 340 (170 per hemisphere) spatially contiguous, approximately equally sized nodes covering the entire cerebral cortex. The parcellation was resampled into each participant's functional volume space using a projection factor of 0.5, i.e., half way into the cortical sheet. For each participant, we extracted mean pre-processed rsfMRI time series from all nodes and calculated a 340x340 connectivity matrix consisting of the Pearson's *r* correlations between nodal time series. Next, we Fisher-transformed all participants' connectivity matrices, and averaged across participants to create a "grand average" connectivity matrix on which network analysis was performed. The grand average connectivity matrix was thresholded at 5, 6, 7, 8, 9, 10, 15, and 20% edge densities. For all thresholded weighted graphs, the optimal modular resolution parameter (gamma) promoting stable decomposition results, was calculated using the Versatility approach (Shinn et al. 2017; see SFig1). Next, modular decomposition was performed with the Louvain algorithm (Blondel et al. 2008) as implemented in the Brain Connectivity Toolbox (BCT) (Rubinov and Sporns 2010) and followed by consensus clustering (Sporns and Betzel 2016). Briefly, this involved calculating an agreement matrix from 10000 independent Louvain partitions, thresholding this empirical agreement matrix by the maximum agreement observed over 10000 randomly generated null association matrices and running clustering on the thresholded empirical agreement matrix. In the case of singleton partitions, i.e., network modules consisting of one node only

– typically consisting of low signal-to-noise regions such as the temporal pole and orbitofrontal cortex – these modules were excluded from the remaining network analyses. Finally, we used the thresholded graphs' optimal community structures to calculate two nodal network measures per graph: *participation coefficient* and *within-module degree*, representing a node's intermodular and intramodular centrality, respectively (Rubinov and Sporns 2010). Two additional measures not requiring information about the underlying community structures were also calculated: *betweenness centrality*, representing the fraction of all shortest paths in the network that contains a given node, and *strength*, the sum of a given node's connectivity weights to every other node (Rubinov and Sporns 2010). Relationships between nodal network measures and estimates of evolutionary expansion were investigated using nonparametric Spearman correlations due to non-normal distributions (assayed using Q-Q plots).

Community density analyses

To investigate high-expanding nodes' anatomical centrality, we used a parcellation of human cortical intrinsic connectivity into 17 canonical networks, estimated from 1000 participants (Yeo et al. 2011). First, we extracted MNI-coordinates for every vertex in the right hemisphere in a downsampled Freesurfer surface representation (fsaverage5; 10242 vertices). Next, for each vertex, we counted the number of canonical networks present within a radius of 5, 10, 15, 20, 25, and 30mm (Euclidean distance). For each radius, the number of networks at every vertex was normalized (0-1) by the maximum number of networks found across all vertices (Power et al. 2013). Finally, the normalized community density values were averaged across radii at each vertex, and correlated with evolutionary

expansion estimates at the same locations using Spearman correlations (due to non-normal distributions).

Flexibility analyses

The functional flexibility of each vertex on the cortical surface of the right hemisphere was estimated from publicly available data (https://surfer.nmr.mgh.harvard.edu/fswiki/BrainmapOntology_Yeo2015). Here, an author-topic hierarchical Bayesian model was used to classify 10449 experimental contrasts from fMRI experiments found in the BrainMap database (Fox and Lancaster 2002) into 12 underlying cognitive components and corresponding brain activity patterns (Yeo et al. 2015). Flexibility was defined as the number of cognitive components activating a voxel. To account for non-integer values due to projections from volume to surface space we rounded surface flexibility estimates to the nearest integer. A nonparametric Kruskal-Wallis was used to compare central tendencies in evolutionary expansion across flexibility groups due to unequal variances across groups (significant Bartlett's test: $\chi^2(8) = 3549$, $p < 1e\text{-}10$)

Task-state connectivity

Following preprocessing, volumetric task-fMRI data were brought to fsaverage surface space. Here, for each participant, we extracted mean BOLD time series from all nodes in the custom 340-node cortical parcellation. Next, psychophysiological interaction (PPI) terms representing nodal task-related activity modulations were calculated using the generalized PPI-toolbox for Matlab (McLaren et al. 2012). For each node, this involved: 1) deconvolving the mean BOLD time series into estimates of neural events (Gitelman et al. 2003); 2) setting up a task-regressor representing the combined auditory-visual-motor-event (2s trial

duration, 50 trials per fMRI run) 3) convolving the product of step 1 and 2 with a canonical hemodynamic response function (cHRF). Finally, to establish task-related functional connectivity between nodes, we estimated pairwise interactions between all nodes' PPI-terms (concatenated over runs) using partial correlations. For each pairwise correlation, we controlled for background noise and task stimulation effects using the nodes' mean BOLD time series and the cHRF-convolved task-regressor, respectively. This "correlational PPI" approach has been described in detail elsewhere (Fornito et al. 2012).

State-dependent coupling analyses

A total of 105 adult participants were represented with matrices of functional connectivity obtained from a resting-state and a task-state. First, the individual connectivity matrices were thresholded to contain only edges surviving FDR-correction ($q<.05$). Next, to allow for a comparison of connectivity data from different states, edge-wise connectivity weights were normalized by the average weight in the matrix (Opsahl et al. 2010). After mapping from weights to lengths (inversing the connection-weights matrices), shortest path-lengths were calculated using Dijkstra's algorithm (Dijkstra 1959). A node's closeness centrality was calculated as the inverse of the average of its shortest path-length to every other node. A repeated measures ANOVA with two within-subject factors; "expansion bin" (5 levels) and "state" (2 levels); was performed to compare closeness centrality measures over regions having undergone different amount of expansion in evolution, as a factor of cognitive state. Note that although estimates of functional connectivity from the two states were derived using different approaches (rest: timeseries correlations; task: correlational PPI), both approaches involve calculating the Pearson's correlation coefficient between the regions' ongoing spontaneous BOLD fluctuations during periods of interest. The state comparisons

were also conducted using identical pre-processing and analysis approaches across the states (see "Control Analyses" below).

Analyses of the developmental sample

The developmental sample consisted of the 105 adult participants described in the section "State-dependent coupling analyses" and 46 participants below 18 years of age (see "Human subjects" section). All non-adult participants were preprocessed and analyzed as described for the adult sample. One participant (age 9.3 years) was excluded from the sample due to high levels of motion (mean absolute motion over two task runs > 1.5mm). A significant positive correlation (Spearman's *rho = .37, p < 4e-06)* was found in the remaining developmental sample (N=150) between estimated motion during the task-state (first principal component of mean absolute and relative motion over two task runs, explaining 98.1% of the total variance) and global closeness centrality (average closeness centrality over all 170 nodes, corresponding to the graph theoretical measure global efficiency (Rubinov and Sporns 2010)). This positive correlation between subject motion and global closeness centrality indicated that participants with relatively high levels of motion (which is a characteristic of young samples (Satterthwaite et al. 2012)) also tended to show high estimates of closeness centrality. To allow for comparisons of closeness-centrality estimates across age groups, unbiased by motion at the global level, we therefore standardized (z-scored) the estimates on a within-subject basis before comparing relative coupling differences across groups. This effectively removed all correlations with motion also when investigating high-expanding and lower-expanding cortex separately (Spearman's *rho* calculated over five expansion bins; lowest expansion to highest expansion: -.06, .14, -.04,

.04, -.01; all *p*-values > .09). Furthermore, we included individual estimates of mean absolute and relative motion as covariates in all statistical tests.

To compare relative coupling across age groups, a repeated measures ANOVA was run with one within-subject factor: "expansion bin" (5 levels), and one between-subject factor: "age group" (2 levels). Mean absolute and relative motion over two task runs were included as covariates. Next, for all 150 participants in the developmental sample, we calculated task-state closeness centrality for each of the 170 nodes in the custom right hemisphere neocortical parcellation and correlated these with evolutionary expansion estimates for the same nodes. We then fitted a nonparametric local smoothing model minimizing the Bayesian information criterion (BIC) to delineate the age trajectory of the relationship between closeness centrality and evolutionary expansion (Fjell et al. 2010). Note that the BIC of the optimal smoothing spline was 8.7 lower than the BIC of a linear fit, indicating that the age trajectories were curvelinear. Confidence intervals of the fit were established using bootstrapping.

Scores on the matrix reasoning and vocabulary subtests of the Wechsler's Abbreviated Scale of Intelligence (WASI; Wechsler 1999) were available from 140 of the participants in the developmental sample (age range 7-38 years). Principal component analysis was run on the raw scores of the two subtests, and the first component, which explained 95.5% of the total variance, was used as a representative measure of general intelligence across participants.

Weighting by Euclidean distance

Euclidean distance between nodes in the right hemisphere was calculated as the average distance (in mm) between the locations of their constituent vertices converted to MNI305 space. To calculate the weighted connectivity matrices, the Euclidean distance matrix was normalized to fall between 0 and 1 and multiplied, element-by-element, with the connectivity matrices across states and participants. Such weighting by geometric distance has been shown to increase sensitivity in detecting graded network differences (Liu et al., 2014), and was applied in all analyses performed on the single-subject level involving comparisons between states or individuals (i.e., the state-dependent coupling analyses (Fig.2), and the analyses of the developmental sample (Fig. 3)). As the network analyses of the rsfMRI data (Fig. 1b) were performed on the grand-average graph and required community detection steps (for which distance weighting would produce networks not comparable to those typically shown in the literature), we conducted these analyses on unweighted data. However, for comparison, the correlations between nodal evolutionary expansion and graph metrics following weighting by Euclidean distance are shown in SFig. 2.

Control analyses

Three series of additional control analyses were carried out to test whether the observed effects were consistent across different analytic choices. First, we performed the state-dependent coupling analyses on edge weights directly, i.e. avoiding the step of mapping weights to lengths. Rather than estimating *closeness centrality*, here we conceptualized a node's centrality as its average correlation to all other nodes in the parcellation (see SFig. 6B). SFig. 7B depicts the same analyses performed on data not weighted by Euclidean distance between nodes.

In a second set of control analyses, we estimated task-state functional connectivity using time-series correlations rather than correlational PPI. Here, data from both task-state runs were preprocessed and analyzed in a similar fashion as the resting-state data. This resulted in two functional connectivity graphs (one per run) per participant, which were averaged before being compared with the resting-state data (see SFig. 6C and the associated caption). SFig. 7C depicts the same analyses performed on data not weighted by Euclidean distance between nodes.

The third set of control analyses involved the regression of motion estimates (mean absolute and relative motion) from the functional connectivity graphs in the developmental sample before comparing relative coupling of high-expanding nodes across age groups. Regression was performed across subjects at the edge-level (i.e., all region-to-region connectivity estimates were corrected). The relevant results following motion regression are shown in SFig. 8.

Across all presented analyses, all tests were two-tailed.

Results

High-expanding cortex has broad functional connections and is engaged flexibly across different cognitive tasks

First, we tested whether high-expanding nodes communicate more broadly across human functional brain networks than low-expanding nodes. Investigations in the macaque monkey have demonstrated strong positive relationships between dendritic complexity at the microscale neuronal level, and broadness of cortico-cortical neuronal connectivity profiles at the macroscale network level (Scholtens et al. 2014). Therefore, we tested whether high-expanding nodes are characterized by high *participation coefficients*, a graph theoretical measure that quantifies the degree to which a node participates in many of the brain's subnetworks (Guimerà and Nunes Amaral 2005). Functional connectivity between nodes covering the entire cerebral cortex was calculated from resting-state functional MRI (rsfMRI) data from 221 healthy young adults. We estimated optimal community structures, i.e. the brain's subnetworks, through modular decomposition of the group-averaged connectivity graph thresholded at different edge densities (SFig. 1a&b). Next, for each threshold, we calculated every node's participation coefficient – a high value indicating that it connects functionally outside its own community. Finally, we extracted average nodal expansion between three non-human simian primates and humans from estimates of evolutionary cortical scaling (Chaplin et al. 2013) (Fig. 1a). A positive relationship was found between nodal participation coefficient values and estimates of evolutionary expansion at all edge densities (Fig. 1b and SFig. 1c), suggesting that high-expanding regions function as integrative connector nodes in the information flow between more specialized modules in human cortex (Power et al. 2013). In line with this observation, nodal *betweenness centrality*

364 also correlated positively with expansion (SFig. 1c), demonstrating that high-expansion
365 regions often participate in the shortest, most efficient, functional path between any two
366 other nodes in the brain network (Rubinov and Sporns 2010).
367
368 Next, we tested whether the topologically broad and central functional connectivity profiles
369 of high-expanding nodes – as indicated by high participation coefficient and betweenness
370 centrality, respectively – were reflected in their anatomical centrality relative to the
371 canonical functional networks of the human brain (Yeo et al. 2011). The measure *community*
372 *density* represents the number of different networks present within a given radius from a
373 cortical location (Power et al. 2013). We observed a positive relationship between local
374 surface expansion and community density, indicating that high-expanding parts of the cortex
375 have access to multiple networks present in their immediate vicinity (Fig. 1c). This closeness,
376 both at the anatomical and the network topology-level, between high-expanding parts of
377 the cortex and the brain's different networks, makes high-expanding cortex ideally situated
378 to engage in a variety of cognitive processes. To test this hypothesis, we took advantage of
379 recent work on the BrainMap database, in which data from ≈10.000 fMRI-experiments have
380 been merged to establish brain activity patterns common to specific types of tasks (Yeo et al.
381 2015). We grouped cortical surface locations based on the number of task-types (“cognitive
382 components”) they were associated with, and then compared expansion across these levels
383 of cognitive flexibility. In line with our hypothesis, highly flexible nodes were found
384 predominantly in high-expanding cortex (Fig. 1d).
385
386

High-expanding cortex communicates preferentially with regions engaged by the current cognitive demands

The above findings suggest that a key role of high-expanding cortical regions may be integration of different cognitive processes. To test this proposal directly, we estimated the *closeness centrality* of cortical nodes in 105 participants scanned using fMRI during two states: unconstrained rest, and a task-state requiring audio-visuo-motor processing (SFig. 3). Closeness centrality represents the average shortest path-length from one node to all other nodes in a network, and thus indicates how tight the functional coupling of a node is to the rest of the network (Rubinov and Sporns 2010). High-expanding regions showed higher closeness centrality during the task-state than during rest and were also more tightly coupled to the rest of the network than lower-expanding nodes (Fig. 2a). Critically, this was also true when accounting for physical (Euclidean) distance between nodes, demonstrating that the tight functional coupling of high-expanding nodes to the rest of the network during multimodal integration is independent of their physical locations on the cortical surface (Liu et al. 2014) (SFig. 4). The higher closeness centrality during the task-state was distributed across all high-expanding regions (Fig. 2b), suggesting that stronger functional coupling during effortful task-operations is a general property of high-expanding cortex and not driven by a subset of cortical regions.

To test the key proposal that evolutionary high-expanding cortex play a central role in *supramodal* cognition – and thus interact flexibly with different parts of cortex depending on particular cognitive demands – we calculated functional coupling change (resting-state to task-state) between high-expanding regions and all cortical nodes. During the multimodal task-state, their coupling increased (i.e. path length decreased) most prominently with

411 posterior visual perceptual regions, auditory cortex and motor cortex (Fig. 2c). In support of
412 the hypothesis that high-expanding cortex connects with regions engaged during a given
413 cognitive state, these regions also showed upregulated functional coupling between
414 themselves during the task state when compared with rest (Fig. 2d). Critically, medial
415 temporal cortex and ventromedial prefrontal cortex, regions found to be involved in
416 memory consolidation processes during offline rest (van Kesteren et al. 2010; Euston et al.
417 2012), showed the opposite pattern: stronger functional coupling with high-expanding
418 cortex during rest than during the task state (Fig. 2c). Moreover, and in direct accordance
419 with the proposal that evolutionary high-expanding cortex interact flexibly with regions
420 engaged in a given cognitive state, functional coupling between these regions was
421 upregulated during rest when compared with the task-state (Fig. 2d).
422
423 **Human development of neocortical functional coupling patterns follows evolutionary**
424 **expansion trajectories**
425 Recent investigations of neocortical morphometry have found similarities between cortical
426 expansion in human development and primate evolution (Fjell et al. 2015). Evolutionary
427 high-expanding cortex, in particular, shows protracted development, and undergoes larger
428 increases in surface area between infancy and adulthood than lower-expanding regions (Hill
429 et al. 2010; Amlien et al. 2016). Notably, this pattern of surface change during development
430 is more pronounced in high-intelligence samples (Schnack et al. 2015), lending support to
431 the idea that similar developmental and evolutionary trajectories of neocortical change –
432 albeit at very different scales – may promote the same phenotypic characteristics of higher
433 intellectual abilities and supramodal cognition.
434

To test whether such correspondence exists between neocortical evolution and functional supramodal cognition characteristics in human cortical development, we collected task-state fMRI data from 46 children and adolescents (6-17 years of age, one excluded due to excessive motion), and compared closeness centrality estimates from regions differing in evolutionary expansion. As found in the adult sample, high-expanding regions' closeness centrality was higher during the multimodal task state also in the children when compared with lower-expanding parts of cortex (Fig. 3a). Additionally, an interaction was observed between age group and regional expansion, indicating that the relative coupling differences between higher- and lower-expanding regions change during development. Specifically, high-expanding cortex' closeness centrality relative to the typical (average) centrality across all nodes, i.e. its relative coupling, was found to be less developed in the young sample when compared with the adults (Fig. 3a). Importantly, less-expanding regions did not show significant differences in coupling between the two age groups. This observation fits well with recent reports of protracted surface area development of evolutionary high-expanding regions, reaching maximum expansion in adolescence (Amlien et al. 2016; Walhovd et al. 2016), and suggests that their roles as multimodal integrating hubs follow related developmental trajectories.

Finally, if evolutionary factors have shaped ontogenetic cortical development, we would expect the mature human brain to reflect the changes that have occurred in primate evolution to a higher degree than the immature brain (e.g. Rakic 2009). For all 150 participants in the adult and development sample, we calculated task-state closeness centrality for each of the 170 nodes in the custom neocortical parcellation and correlated these with evolutionary expansion estimates for the same nodes. Next, we fitted a

nonparametric local smoothing model (Fjell et al. 2010) to delineate the age trajectory of the relationship between closeness centrality and evolutionary expansion. The relationship was found to be not significant until approximately eighteen years of age, at which point the fit revealed positive correlations between neocortical functional coupling pattern and expansion (Fig. 3b). Interestingly, and in line with previous morphometric reports (Fjell et al. 2015; Schnack et al. 2015), participants showing higher similarity between their nodal centrality maps and the evolutionary expansion map were characterized by higher scores on measures of general intelligence (Fig. 3c). This suggests that evolutionary concepts resonating in the functional coupling of the human neocortex are relevant for the characteristic human phenotype of higher intellectual function.

Control analyses

The control analyses (presented in SFig. 6-8) supported the main findings reported above. One discrepancy was however observed: when analyzing task data following the resting-state analysis approach (SFig 6C+7C), we did not observe stronger coupling between high-expanding cortex and medial temporal / ventromedial prefrontal cortex during rest when compared to the multimodal task-state. We suspect this may be due to the task time series also containing long periods of rest during the inter-trial intervals. While these inter-trial rest periods were effectively excluded in the main analyses using the correlational PPI approach, they remained present in the control analyses since functional connectivity here was defined as correlations between BOLD time-series covering the full task runs, i.e. without discriminating between state changes within the runs.

Discussion

Our findings point to a central role of evolutionary high-expanding cortex in integrative operations during a variety of cognitive states. The functional signature of such supramodal cognition matures throughout childhood, suggesting that the high-expanding regions develop their characteristic of broad functional connections to many of the brain's networks in tandem with the emergence and refinement of central human cognitive skills. Their postulated overarching function in facilitating supramodal and flexible cognition is supported by the reported links between general intelligence and surface area of high-expanding regions (Fjell et al. 2015; Schnack et al. 2015). Moreover, the functional connectivity 'fingerprints' of high-expanding cortex have been shown to be highly variable from participant to participant, and these characteristic overlaps well with the degree to which a brain region can be used to predict performance during different types of cognition (Mueller et al. 2013). The underlying cellular machinery appears optimized to support such supramodal processes: neuromorphological investigations of primate cortex have found more elaborate dendritic layouts in high-expanding compared with low-expanding regions (Elston et al. 1999), and these structural properties are more pronounced in humans than in non-human primates (Bianchi et al. 2013; Geschwind and Rakic 2013; Donahue et al. 2018).

In the current study, we interpret cortical regions demonstrating the capacity to integrate information from across the brain in a flexible manner as to take part in supramodal cognition. The claim that certain parts of the cortex, and in particular prefrontal regions, play such flexible integrative roles is hardly new (e.g., Goldman-Rakic 1988), however we believe there is novelty in linking these broad functions to evolutionary morphological changes and

504 their candidate behavioral phenotypes. Our results suggest that, when analyzed as a unit,
505 high-expanding cortex shows both integrative and supramodal characteristics. However, the
506 regions constituting the expansion 'hotspots' are spread in a partly discontinuous manner
507 across large portions of the cortex and may show different characteristics and specializations
508 when investigated in a more fine-grained fashion (Chaplin et al. 2013). A fascinating venue
509 for further research could be to collect data on unimodal in addition to multimodal tasks in
510 an attempt to disentangle modality-specific from integrative functions. Specifically, regions
511 showing increased task-related recruitment and/or functional coupling during multimodal
512 states when compared to unimodal states could be said to be integrative, while regions
513 demonstrating differential coupling patterns over varying task-requirements would support
514 supramodal flexibility. The current results suggest that one would find regions fulfilling both
515 criteria primarily within evolutionary high-expanding cortex.
516
517 **Methodological considerations and limitations**
518 While measures of functional connectivity may be reflective of underlying anatomical
519 connectivity (Vincent et al. 2007; Honey et al. 2009; Hermundstad et al. 2013), they are
520 nevertheless estimated from covariations in signal time-series and can thus be affected by
521 mechanisms other that direct interactions between neuronal populations. In the current
522 study, we do not base any conclusions on observations from single edges (i.e., simple
523 bivariate correlations between two regions), but rely on graph theoretical nodal summary
524 measures – such as closeness centrality – and regions' relative roles in the brain network
525 along these measures. Moreover, due to the within-subject nature of our coupling analyses,
526 we base our conclusions about high-expanding cortex and supramodality on the observed
527 consistent *modulations* in functional coupling across states, not the presence/absence of

specific connections. It should be stressed that path-based graph metrics, when estimated from functional connectivity networks, are statistical constructs that do not necessarily reflect information flow along anatomical connections in the brain (Rubinov & Sporns, 2010; Smith et al., 2013; Fornito et. al, 2016). The successful use of functional path-length measures as predictors of cognition (e.g., Bassett et al., 2009; van den Heuvel et al., 2009; Kinnison et al., 2012), and observations that such metrics are under genetic control (Fornito et al., 2011; van den Heuvel et al., 2013; Sinclair et al., 2015), suggests that they reflect biologically meaningful processes and network characteristics. At present, however, shortest path-length measures derived from correlation-based functional networks should not be considered as direct anatomical links. In the current study, we observe similar effects when calculating coupling based on raw correlation weights rather than path-length measures (SFig. 6B and 7B). While this suggests that the observed strong centrality of evolutionary high-expanding regions during multimodal cognitive operations is not an artefact of converting weights to lengths, edge-correlation weights have limited interpretability in terms of anatomical pathways as they can reflect both direct couplings between nodes and interactions via intermediate regions (Fornito et al., 2016).

Some uncertainty is also associated with the reported relationship between nodal participation coefficient and evolutionary expansion (i.e., Fig. 1b) as they were derived from group averaged graphs of functional connectivity and network parcellations of these. Interestingly, recent work on individual-specific network parcellations (e.g., Gordon et al., 2017; Kong et al., 2018) have suggested that the size, location, and spatial arrangement of cortical networks differ (to some degree) between participants. A common observation in these studies seems to be higher intersubject variability in the spatial layout of association

552 networks when compared with sensory-/motor-networks (Laumann et al., 2015; Wang et al.,
553 2015; Kong et al., 2018), in line with the idea that the development of areas in these
554 networks is less constrained by molecular specification steps in early development (Rosa and
555 Tweedale 2005). In principle, the high participation coefficients observed in high-expanding
556 association cortex when calculated from the group averaged graphs – indicating strong
557 functional coupling across networks – could thus in part be reflective of heterogeneity in the
558 network profiles at the individual level. We are not, however, aware that there is any
559 consensus about how to navigate between individual-specific and group-level based
560 network parcellations and interpret the observed topographical discrepancies. As reliable
561 estimates of the participation coefficient at the individual level are hard to establish even
562 with extensive periods of resting-state data per participant (Gordon et al., 2017), we have
563 here tried to take an alternative approach by investigating high-expanding cortex' postulated
564 integrative role using a variety of measures and approaches. Thus, while keeping the
565 important limitations discussed above in mind, we believe our general claims are supported
566 and strengthened by the observed consistencies across modalities (Community Density
567 analyses) and with independent datasets (Flexibility analyses), as well as by the replication of
568 selective increase in high-expanding cortex' functional coupling during multimodal
569 requirements across two independent groups of participants (Developmental Sample
570 analyses).
571
572 The observed correlations between our measures of functional coupling and registered head
573 motion in the developmental sample were mitigated through standardization at the
574 individual data level, and by including individual motion estimates as covariates at the
575 statistical level. Per-individual standardization of closeness centrality coupling measures

effectively removed potential global effects of motion (i.e., affecting all regions) on the centrality measures. Importantly, the standardization step also removed all observed significant correlations between motion and centrality measures when investigating regions characterized by different amounts of evolutionary expansion – "expansion bins" – separately. In other words, after removing potential global effects of head motion from the data, no correlation was found between individual differences in functional coupling of high-expanding cortex and motion (nor for any other expansion bin). Nevertheless, we included an additional control analysis in which motion estimates across subjects were aggressively regressed in an edge-wise fashion from the participant graphs in the developmental sample. While the effects reported in Fig. 3a were only marginally influenced by this additional data cleaning step (see SFig. 8), it should be noted that the correction likely affected shared variance between motion and age-normalized participant IQ (Spearman's *rho* = -.24, *p* = .005), and participant age (Spearman's *rho* = -.39; *p* = 7.3e-07), that is, variables found to be associated with the function and development of high-expanding cortex (Hill et al., 2010; Schnack et al. 2015).

The present study is based on interpretation of functional data obtained in humans, correlated with estimates of the differential expansion of parts of the cerebral cortex in primate evolution. To date, these estimates have been derived from careful histological reconstruction of single individual brains from different species, followed by computational registration of 3-dimensional models (Chaplin et al. 2013). The reliance of these estimates on individual brains, rather than population averages, represents a possible limitation of the precision of the present analyses. It should be noted, however, that the differences in expansion that underlie our conclusions are very substantial, relative to the likely degree of

individual variation, or errors derived from incorrect assignment of cytoarchitectural boundaries. For example, the differential expansion between the most notable expansion 'hotspots' (temporoparietal junction, ventrolateral prefrontal cortex, and dorsal anterior cingulate cortex) and other regions, such as the primary visual cortex and parahippocampal gyrus, is as high as 16-fold between macaque and human (Hill et al. 2010), which is well beyond the variation observed in the volumes of cytoarchitectural areas between individuals of a single primate species (cf. Majka et al. 2016; Woodward et al. 2018). Moreover, although quantitative details of the expansion of different cortical nodes vary slightly depending on which species are used for comparison, the locations of the expansion 'hotspots' are remarkably stable (Chaplin et al. 2013). Finally, although some controversy remains about the relative expansion of some regions of the cerebral cortex in primate evolution (e.g. frontal lobe; Barton and Venditti 2013; Sherwood and Smaers 2013), it must be noted that the estimates used in the present study are based on quantitative analyses of species to species registration that took into consideration cytoarchitectural boundaries of areas that are well-defined, rather than gross morphological features of the brain; recent studies that also used cytoarchitecture to guide registration have confirmed that differential expansion exists (Mansouri et al. 2017; Donahue et al. 2018).

Conclusion

The present results add to existing knowledge by showing how evolutionary high-expanding regions change in their role as communication hubs in different cognitive states, and that this power gradually emerges during childhood and adolescence development.

Funding

This work was supported by the Norwegian Research Council (grants to A.M.F and K.B.W.), the European Research Council Starting Grant and Consolidator Grant scheme under grant agreements 283634 and 725025 (to AMF) and 313440 (to KBW), as well as the Department of Psychology, University of Oslo (to K.B.W., A.M.F.). The comparative data were obtained with funding of the Australian Research Council.

Acknowledgements:

We would like to thank Ed Bullmore (University of Cambridge) for helpful comments on an earlier draft of the manuscript, and Didac Vidal Piñeiro (University of Oslo) for help with analyses. The authors declare no competing interests.

References

Amlien IK, Fjell AM, Tamnes CK, Grydeland H, Krogsrud SK, Chaplin TA, Rosa MGP, Walhovd KB. 2016. Organizing Principles of Human Cortical Development - Thickness and Area from 4 to 30 Years: Insights from Comparative Primate Neuroanatomy. Cereb Cortex. 26:257–267.

Barton RA, Venditti C. 2013. Human frontal lobes are not relatively large. Proc Natl Acad Sci. 110:9001–9006.

Bassett DS, Bullmore ET, Meyer-Lindenberg A, Apud JA, Weinberger DR, Coppola R. 2009. Cognitive fitness of cost-efficient brain functional networks. Proc Natl Acad Sci. 106:11747–11752.

Bianchi S, Stimpson CD, Bauernfeind AL, Schapiro SJ, Baze WB, McArthur MJ, Bronson E, Hopkins WD, Semendeferi K, Jacobs B, Hof PR, Sherwood CC. 2013. Dendritic morphology of pyramidal neurons in the chimpanzee neocortex: regional specializations and comparison to humans. Cereb Cortex. 23:2429–2436.

Blondel VD, Guillaume J-L, Lambiotte R, Lefebvre E. 2008. Fast unfolding of communities in large networks. J Stat Mech Theory Exp. 10008:6.

Buckner RL, Krienen FM. 2013. The evolution of distributed association networks in the human brain. Trends Cogn Sci. 17:648–665.

Chaplin TA, Yu H-H, Soares JGM, Gattass R, Rosa MGP. 2013. A Conserved Pattern of Differential Expansion of Cortical Areas in Simian Primates. J Neurosci. 33:15120–15125.

Craddock RC, James GA, Holtzheimer PE, Hu XP, Mayberg HS. 2012. A whole brain fMRI atlas generated via spatially constrained spectral clustering. Hum Brain Mapp. 33:1914–

1928.

Dijkstra EW. 1959. A note on two problems in connexion with graphs. Numer Math. 1:269–271.

Donahue CJ, Glasser MF, Preuss TM, Rilling JK, Van Essen DC. 2018. Quantitative assessment of prefrontal cortex in humans relative to nonhuman primates. Proc Natl Acad Sci U S A. 201721653.

Elston GN, Tweedale R, Rosa MGP. 1999. Cortical integration in the visual system of the macaque monkey: large-scale morphological differences in the pyramidal neurons in the occipital, parietal and temporal lobes. Proc R Soc B Biol Sci. 266:1367–1374.

Euston DR, Gruber AJ, McNaughton BL. 2012. The role of medial prefrontal cortex in memory and decision making. Neuron. 76:1057–1070.

Finlay BL, Darlington RB. 1995. Linked regularities in the development and evolution of mammalian brains. Science. 268:1578–1584.

Fjell AM, Walhovd KB, Westlye LT, Østby Y, Tamnes CK, Jernigan TL, Gamst A, Dale AM. 2010. When does brain aging accelerate? Dangers of quadratic fits in cross-sectional studies. Neuroimage. 50:1376–1383.

Fjell AM, Westlye LT, Amlien I, Tamnes CK, Grydeland H, Engvig A, Espeseth T, Reinvang I, Lundervold AJ, Lundervold A, Walhovd KB. 2015. High-expanding cortical regions in human development and evolution are related to higher intellectual abilities. Cereb Cortex. 25:26–34.

Fonseca-Azevedo K, Herculano-Houzel S. 2012. Metabolic constraint imposes tradeoff between body size and number of brain neurons in human evolution. Proc Natl Acad Sci U S A. 109:18571–18576.

Fornito A, Zalesky A, Bassett DS, Meunier D, Ellison-Wright I, Yucel M, Wood SJ, Shaw K,

O'Connor J, Nertney D, Mowry BJ, Pantelis C, Bullmore ET. 2011. Genetic Influences on Cost-Efficient Organization of Human Cortical Functional Networks. J Neurosci. 31:3261–3270.

Fornito A, Harrison BJ, Zalesky A, Simons JS. 2012. Competitive and cooperative dynamics of large-scale brain functional networks supporting recollection. Proc Natl Acad Sci U S A. 109:12788–12793.

Fornito A, Zalesky A, Bullmore ETBT-F of BNA (Eds.). 2016. Chapter 7 - Paths, Diffusion, and Navigation. In: Fundamentals of Brain Network Analysis. San Diego: Academic Press. p. 207–255.

Fox PT, Lancaster JL. 2002. Opinion: Mapping context and content: the BrainMap model. Nat Rev Neurosci. 3:319–321.

Geschwind DH, Rakic P. 2013. Cortical evolution: Judge the brain by its cover. Neuron. 80:633–647.

Gitelman DR, Penny WD, Ashburner J, Friston KJ. 2003. Modeling regional and psychophysiologic interactions in fMRI: the importance of hemodynamic deconvolution. Neuroimage. 19:200–207.

Goldman-Rakic PS. 1988. Topography of cognition: parallel distributed networks in primate association cortex. Annu Rev Neurosci. 11:137–156.

Gordon EM, Laumann TO, Gilmore AW, Newbold DJ, Greene DJ, Berg JJ, Ortega M, Hoyt-Drazen C, Gratton C, Sun H, Hampton JM, Coalson RS, Nguyen AL, McDermott KB, Shimony JS, Snyder AZ, Schlaggar BL, Petersen SE, Nelson SM, Dosenbach NUF. 2017. Precision Functional Mapping of Individual Human Brains. Neuron. 95:791–807.e7.

Guimerà R, Nunes Amaral LA. 2005. Functional cartography of complex metabolic networks. Nature. 433:895–900.

Hallquist MN, Hwang K, Luna B. 2013. The Nuisance of Nuisance Regression: Spectral Misspecification in a Common Approach to Resting-State fMRI Preprocessing Reintroduces Noise and Obscures Functional Connectivity. Neuroimage. 82C:208–225.

Herculano-Houzel S. 2011. Scaling of brain metabolism with a fixed energy budget per neuron: implications for neuronal activity, plasticity and evolution. PLoS One. 6:e17514.

Herculano-Houzel S. 2012. The remarkable, yet not extraordinary, human brain as a scaled-up primate brain and its associated cost. Proc Natl Acad Sci. 109:10661–10668.

Hermundstad AM, Bassett DS, Brown KS, Aminoff EM, Clewett D, Freeman S, Frithsen A, Johnson A, Tipper CM, Miller MB, Grafton ST, Carlson JM. 2013. Structural foundations of resting-state and task-based functional connectivity in the human brain. Proc Natl Acad Sci U S A. 110:6169–6174.

Hill J, Inder T, Neil J, Dierker D, Harwell J, Van Essen D. 2010. Similar patterns of cortical expansion during human development and evolution. Proc Natl Acad Sci U S A. 107:13135–13140.

Honey CJ, Honey CJ, Sporns O, Sporns O, Cammoun L, Cammoun L, Gigandet X, Gigandet X, Thiran JP, Thiran JP, Meuli R, Meuli R, Hagmann P, Hagmann P. 2009. Predicting human resting-state functional connectivity from structural connectivity. Proc Natl Acad Sci U S A. 106:2035–2040.

Kinnison J, Padmala S, Choi J-M, Pessoa L. 2012. Network Analysis Reveals Increased Integration during Emotional and Motivational Processing. J Neurosci. 32:8361–8372.

Kong R, Li J, Orban C, Sabuncu MR, Liu H, Schaefer A, Sun N, Zuo X-N, Holmes AJ, Eickhoff SB, Yeo BTT. 2018. Spatial Topography of Individual-Specific Cortical Networks Predicts Human Cognition, Personality, and Emotion. Cereb Cortex. 1–19.

Krienen FM, Yeo BTT, Buckner RL. 2014. Reconfigurable task-dependent functional coupling

728 modes cluster around a core functional architecture. Philos Trans R Soc Lond B Biol Sci.
729 369.
730 Laumann TO, Gordon EM, Adeyemo B, Snyder AZ, Joo SJ un, Chen MY, Gilmore AW,
731 McDermott KB, Nelson SM, Dosenbach NUF, Schlaggar BL, Mumford JA, Poldrack RA,
732 Petersen SE. 2015. Functional System and Areal Organization of a Highly Sampled
733 Individual Human Brain. Neuron. 87:657–670.
734 Liu Y, Yu C, Zhang X, Liu J, Duan Y, Alexander-Bloch AF, Liu B, Jiang T, Bullmore E. 2014.
735 Impaired long distance functional connectivity and weighted network architecture in
736 alzheimer's disease. Cereb Cortex. 24:1422–1435.
737 Majka P, Chaplin TA, Yu HH, Tolpygo A, Mitra PP, Wójcik DK, Rosa MGP. 2016. Towards a
738 comprehensive atlas of cortical connections in a primate brain: Mapping tracer
739 injection studies of the common marmoset into a reference digital template. J Comp
740 Neurol. 524:2161–2181.
741 Mansouri FA, Koechlin E, Rosa MGP, Buckley MJ. 2017. Managing competing goals - A key
742 role for the frontopolar cortex. Nat Rev Neurosci. 18:645–657.
743 McLaren DG, Ries ML, Xu G, Johnson SC. 2012. A generalized form of context-dependent
744 psychophysiological interactions (gPPI): a comparison to standard approaches.
745 Neuroimage. 61:1277–1286.
746 Mueller S, Wang D, Fox MD, Yeo BTT, Sepulcre J, Sabuncu MR, Shafee R, Lu J, Liu H. 2013.
747 Individual Variability in Functional Connectivity Architecture of the Human Brain.
748 Neuron. 77:586–595.
749 Opsahl T, Agneessens F, Skvoretz J. 2010. Node centrality in weighted networks:
750 Generalizing degree and shortest paths. Soc Networks. 32:245–251.
751 Power JD, Schlaggar BL, Lessov-Schlaggar CN, Petersen SE. 2013. Evidence for hubs in human

752 functional brain networks. Neuron. 79:798–813.
753 Pruim RHR, Mennes M, Buitelaar JK, Beckmann CF. 2015. Evaluation of ICA-AROMA and
754 alternative strategies for motion artifact removal in resting-state fMRI. Neuroimage.
755 112:278–287.
756 Rakic P. 2009. Evolution of the neocortex: a perspective from developmental biology. Nat
757 Rev Neurosci. 10:724–735.
758 Rilling JK. 2014. Comparative primate neuroimaging: Insights into human brain evolution.
759 Trends Cogn Sci. 18:46–55.
760 Ringo JL. 1991. Neuronal interconnection as a function of brain size. Brain Behav Evol. 38:1–
761 6.
762 Rosa MGP, Tweedale R. 2005. Brain maps, great and small: lessons from comparative studies
763 of primate visual cortical organization. Philos Trans R Soc Lond B Biol Sci. 360:665–691.
764 Rubinov M, Sporns O. 2010. Complex network measures of brain connectivity: uses and
765 interpretations. Neuroimage. 52:1059–1069.
766 Salimi-Khorshidi G, Douaud G, Beckmann CF, Glasser MF, Griffanti L, Smith SM. 2014.
767 Automatic denoising of functional MRI data: Combining independent component
768 analysis and hierarchical fusion of classifiers. Neuroimage. 90:449–468.
769 Satterthwaite TD, Wolf DH, Loughead J, Ruparel K, Elliott MA, Hakonarson H, Gur RC, Gur RE.
770 2012. Impact of in-scanner head motion on multiple measures of functional
771 connectivity: Relevance for studies of neurodevelopment in youth. Neuroimage.
772 60:623–632.
773 Schnack HG, van Haren NEM, Brouwer RM, Evans A, Durston S, Boomsma DI, Kahn RS,
774 Hulshoff Pol HE. 2015. Changes in Thickness and Surface Area of the Human Cortex and
775 Their Relationship with Intelligence. Cereb Cortex. 25:1608–1617.

776 Scholtens LH, Schmidt R, de Reus MA, van den Heuvel MP. 2014. Linking macroscale graph
777 analytical organization to microscale neuroarchitectonics in the macaque connectome.
778 J Neurosci. 34:12192–12205.
779 Sherwood CC, Smaers JB. 2013. What's the fuss over human frontal lobe evolution? Trends
780 Cogn Sci. 17:432–433.
781 Shinn M, Romero-Garcia R, Seidlitz J, Váša F, Vértes PE, Bullmore E. 2017. Versatility of nodal
782 affiliation to communities. Sci Rep. 7:4273.
783 Sinclair B, Hansell NK, Blokland GAM, Martin NG, Thompson PM, Breakspear M, de Zubicaray
784 GI, Wright MJ, McMahon KL. 2015. Heritability of the network architecture of intrinsic
785 brain functional connectivity. Neuroimage. 121:243–252.
786 Smaers JB, Gómez-Robles A, Parks AN, Sherwood CC. 2017. Exceptional Evolutionary
787 Expansion of Prefrontal Cortex in Great Apes and Humans. Curr Biol. 27:714–720.
788 Smith SM, Vidaurre D, Beckmann CF, Glasser MF, Jenkinson M, Miller KL, Nichols TE,
789 Robinson EC, Salimi-Khorshidi G, Woolrich MW, Barch DM, Uğurbil K, Van Essen DC.
790 2013. Functional connectomics from resting-state fMRI. Trends Cogn Sci. 17:666–682.
791 Sneve MH, Grydeland H, Nyberg L, Bowles B, Amlien IK, Langnes E, Walhovd KB, Fjell AM.
792 2015. Mechanisms Underlying Encoding of Short-Lived Versus Durable Episodic
793 Memories. J Neurosci. 35:5202–5212.
794 Sporns O, Betzel RF. 2016. Modular Brain Networks. Annu Rev Psychol. 67:annurev-psych-
795 122414-033634.
796 Tagliazucchi E, Laufs H. 2014. Decoding Wakefulness Levels from Typical fMRI Resting-State
797 Data Reveals Reliable Drifts between Wakefulness and Sleep. Neuron. 82:695–708.
798 Toro R, Perron M, Pike B, Richer L, Veillette S, Pausova Z, Paus T. 2008. Brain size and folding
799 of the human cerebral cortex. Cereb Cortex. 18:2352–2357.

van den Heuvel MP, Stam CJ, Kahn RS, Hulshoff Pol HE. 2009. Efficiency of functional brain networks and intellectual performance. J Neurosci. 29:7619–7624.

van den Heuvel MP, van Soelen ILC, Stam CJ, Kahn RS, Boomsma DI, Hulshoff Pol HE. 2013. Genetic control of functional brain network efficiency in children. Eur Neuropsychopharmacol. 23:19–23.

Van Essen DC, Drury HA, Dickson J, Harwell J, Hanlon D, Anderson CH. 2001. An integrated software suite for surface-based analyses of cerebral cortex. J Am Med Informatics Assoc. 8:443–459.

van Kesteren MTR, Fernández G, Norris DG, Hermans EJ. 2010. Persistent schema-dependent hippocampal-neocortical connectivity during memory encoding and postencoding rest in humans. Proc Natl Acad Sci U S A. 107:7550–7555.

Vendetti MS, Bunge SA. 2014. Evolutionary and developmental changes in the lateral frontoparietal network: A little goes a long way for higher-level cognition. Neuron. 84:906–917.

Vincent JL, Patel GH, Fox MD, Snyder AZ, Baker JT, Van Essen DC, Zempel JM, Snyder LH, Corbetta M, Raichle ME. 2007. Intrinsic functional architecture in the anaesthetized monkey brain. Nature. 447:83–86.

Vuoksimaa E, Panizzon MS, Chen CH, Fiecas M, Eyler LT, Fennema-Notestine C, Hagler DJ, Franz CE, Jak AJ, Lyons MJ, Neale MC, Rinker DA, Thompson WK, Tsuang MT, Dale AM, Kremen WS. 2016. Is bigger always better? The importance of cortical configuration with respect to cognitive ability. Neuroimage. 129:356–366.

Walhovd KB, Fjell AM, Giedd J, Dale AM, Brown TT. 2016. Through Thick and Thin: a Need to Reconcile Contradictory Results on Trajectories in Human Cortical Development. Cereb Cortex. 1989:bhv301.

824 Wang D, Buckner RL, Fox MD, Holt DJ, Holmes AJ, Stoecklein S, Langs G, Pan R, Qian T, Li K,
825 Baker JT, Stufflebeam SM, Wang K, Wang X, Hong B, Liu H. 2015. Parcellating cortical
826 functional networks in individuals. Nat Neurosci. 18:1853–1860.
827 Wechsler D. 1999. Wechsler abbreviated scale of intelligence. San Antonio, Texas: The
828 Psychological Corporation.
829 Woodward A, Hashikawa T, Maeda M, Kaneko T, Hikishima K, Iriki A, Okano H, Yamaguchi Y.
830 2018. Data descriptor: The Brain/MINDS 3D digital marmoset brain atlas. Sci Data. 5:1–
831 12.
832 Yekutieli D, Benjamini Y. 2001. The control of the false discovery rate in multiple testing
833 under dependency. Ann Stat. 29:1165–1188.
834 Yeo BTT, Krienen FM, Eickhoff SB, Yaakub SN, Fox PT, Buckner RL, Asplund CL, Chee MWLL,
835 Yeo BTT, Krienen FM, Eickhoff SB, Yaakub SN, Fox PT, Buckner RL, Asplund CL, Chee
836 MWLL. 2015. Functional specialization and flexibility in human association cortex. Cereb
837 Cortex. 25:3654–3672.
838 Yeo BTT, Krienen FM, Sepulcre J, Sabuncu MR, Lashkari D, Hollinshead M, Roffman JL,
839 Smoller JW, Zöllei L, Polimeni JR, Fischl B, Liu H, Buckner RL. 2011. The organization of
840 the human cerebral cortex estimated by intrinsic functional connectivity. J
841 Neurophysiol. 106:1125–1165.
842

Figures legends

Figure 1

High-expanding cortex has broad functional connections and is flexibly engaged across different cognitive tasks. (a) Estimates of evolutionary expansion for 170 similarly sized nodes covering the right hemisphere. (b) Spearman correlation between node expansion and node participation coefficient. The presented values are averaged across thresholds and ranked – plotted linear relationship thus represent the Spearman correlation. Observed (non-ranked) participation coefficient values scaled between 0 and 0.71. Traditional hub-measures not incorporating integrative aspects of nodal communication (within-module degree, node strength), did not show any relationships with node expansion (SFig. 1c). (c) Density plot showing the Spearman correlation between vertices' normalized community and estimated evolutionary expansion. (d) Violin plots showing the relationship between cortical expansion and cognitive flexibility at the vertex level. Median expansion is shown as horizontal lines. A Kruskal-Wallis test confirmed that expansion differed across flexibility groups. Post-hoc pairwise comparisons demonstrated that cortical locations involved in five or more cognitive components were more expanded than locations involved in four or less components ($p<1.25e-07$). All reported p-values are corrected for multiple tests.

Figure 2

High-expanding cortex communicates differently depending on the current cognitive demands, and preferentially with regions engaged by those demands. (a) Average closeness centrality for five expansion bins during resting- and task-state (dark blue: 20% least expanding nodes, yellow: 20% most-expanding nodes; intermediate colors: intermediate expansion levels). Following a significant "expansion bin X state" repeated

867 measures ANOVA (Greenhouse-Geisser corrected following a significant Mauchly's test of
868 sphericity: χ^2 (9) = 129, p < 1e-10), paired-samples t-tests showed significant increase in
869 closeness centrality in task- compared to resting-state for the highest-expanding nodes only:
870 t(104)=4.27, p_{FDR} < 5.0e-04. (b) Nodes within expansion hotspot regions (indicated by yellow
871 lines) showing significant (paired-samples t-tests, p_{FDR} < .05) changes in closeness centrality
872 from rest to task. (c) Nodes showing significant change (paired-samples t-tests, p_{FDR} < .05) in
873 functional coupling with expansion hotspots from rest to task across participants. (d) Mean
874 functional coupling between nodes showing negative (blue) / positive effect (yellow) in
875 panel c. Nodes falling within the expansion hotspot regions were excluded when calculating
876 the mean. Nodes more strongly coupled with high-expanding regions during rest (R>T)
877 showed higher coupling with each other during rest than during task: paired-samples t-test,
878 t(104)=-10.56, p_{FDR} < 3.7e-18. The opposite effect was observed between nodes more
879 strongly coupled with high-expanding regions during the task-state (T>R): paired-samples t-
880 test, t(104)=13.25, p_{FDR} < 4.4e-24. The presented data have been weighted by Euclidean
881 distance between nodes. Unweighted data show similar effects (SFig. 6A). All reported p-
882 values are corrected for multiple tests. Error bars represent SEM.
883
884 **Figure 3**
885 **Human development of neocortical multimodal coupling patterns follows evolutionary**
886 **expansion trajectories**. (a) High-expanding cortex showed stronger relative coupling than
887 lower-expanding regions in both age groups (children: t(44)>8.09, p_{FDR} < 3.0e-10; adults:
888 t(104)>23.73, p_{FDR} < 1.0e-10). Following the significant "age group x expansion bin"
889 interaction (Greenhouse-Geisser corrected following a significant Mauchly's test of
890 sphericity: χ^2 (9) = 63.6, p < 3e-10), post hoc tests showed lower relative coupling of high-

891 expanding nodes in the development sample compared to the adults (Z = -2.68, p_{FDR} < .037;
892 Wilcoxon rank sum due to unequal variances across groups: Bartlett's test: χ^2 (1) = 20.8, p <
893 6e-06). Lower-expanding nodes did not show significant differences in relative coupling
894 between age groups (p_{FDR} > .093). Error bars represent SEM. (b) Individual correlation
895 between nodal closeness centrality and evolutionary expansion plotted as a function of age.
896 The black line represents the best fitting smoothing spline. Red lines represent the
897 bootstrapped 95% confidence interval of the fit. Blue dotted line shows the correlation
898 coefficient at which a correlation with 169 degrees of freedom is significant at p < .05
899 (abs(rho) > .151). (c) First principal component calculated from raw scores on two WASI
900 subtests plotted as a function of age. Spearman correlations revealed significant
901 relationships between this measure of general intelligence and individual differences in
902 closeness centrality-vs-expansion correlation (i.e. correlating data points in Fig. 3b and 3c:
903 Spearman's rho = .34, p < 4.9e-5). Importantly, this relationship remained when controlling
904 for nonlinear influences of age using partial Spearman correlations (rho = .184, p = .030), and
905 when including motion estimates (in addition to age) as control variables (rho = .177, p
906 =.039)
907

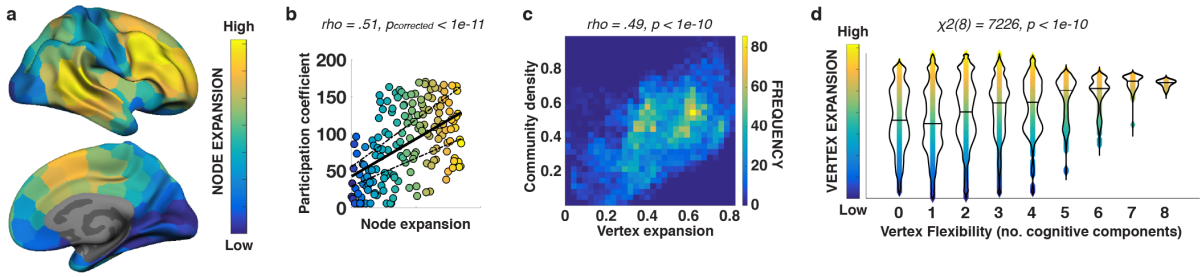
a
High
NODE EXPANSION
Low
b
rho = .51, pcorrected < 1e-11
Participation coefficient
200
150
100
50
0
Node expansion
c
rho = .49, p < 1e-10
Community density
0.8
0.6
0.4
0.2
0
0.2
0.4
0.6
0.8
Vertex expansion
80
60
40
20
0
FREQUENCY
d
High
VERTEX EXPANSION
Low
χ2(8) = 7226, p < 1e-10
0
1
2
3
4
5
6
7
8
Vertex Flexibility (no. cognitive components)

Figure 1

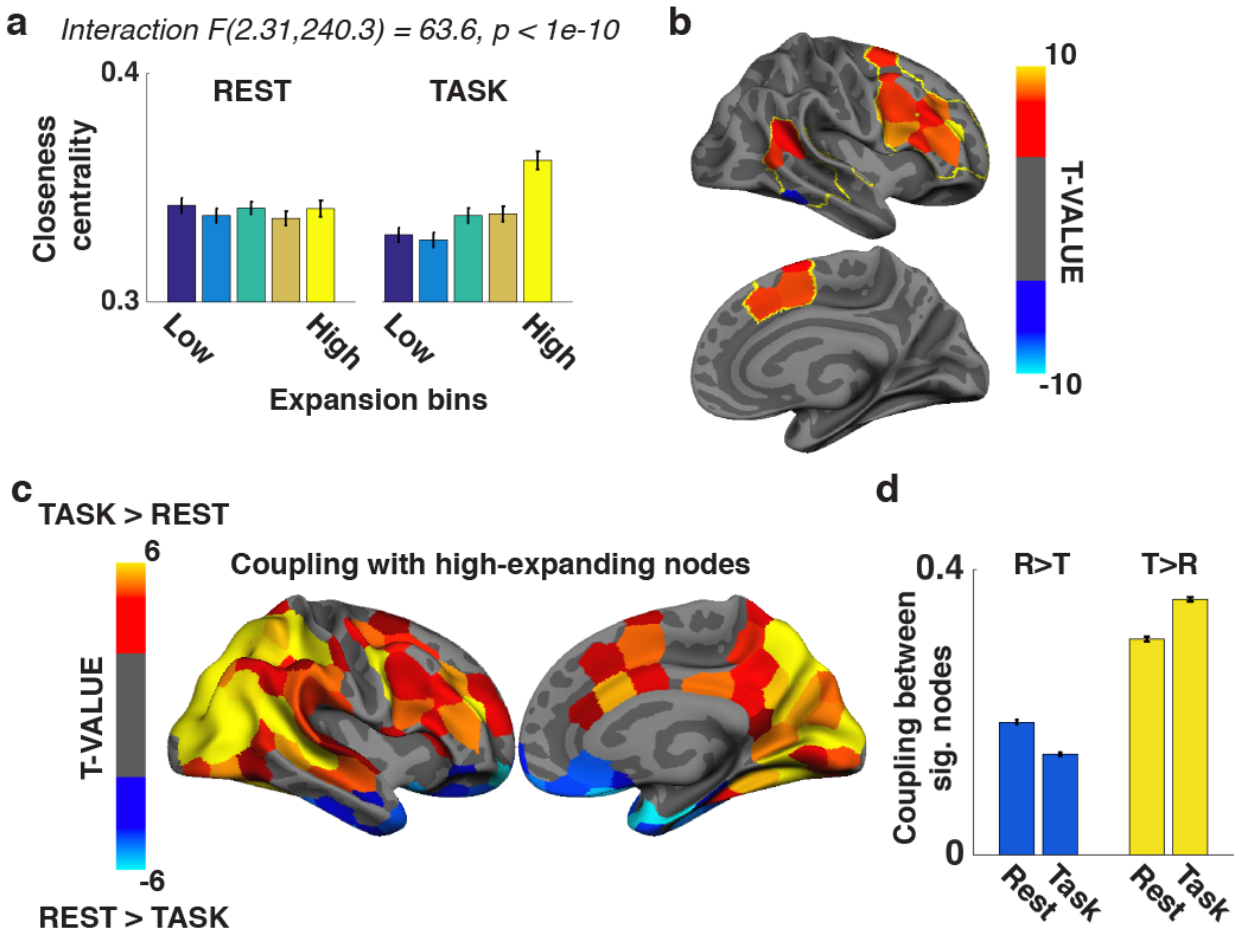
a
Interaction F(2.31,240.3) = 63.6, p < 1e-10
0.4
0.3
Closeness centrality
REST
TASK
Low
High
Low
High
Expansion bins
b
10
T-VALUE
-10
c
TASK > REST
6
T-VALUE
-6
REST > TASK
Coupling with high-expanding nodes
d
0.4
0
Coupling between sig. nodes
R>T
T>R
Rest
Task
Rest
Task

Figure 2

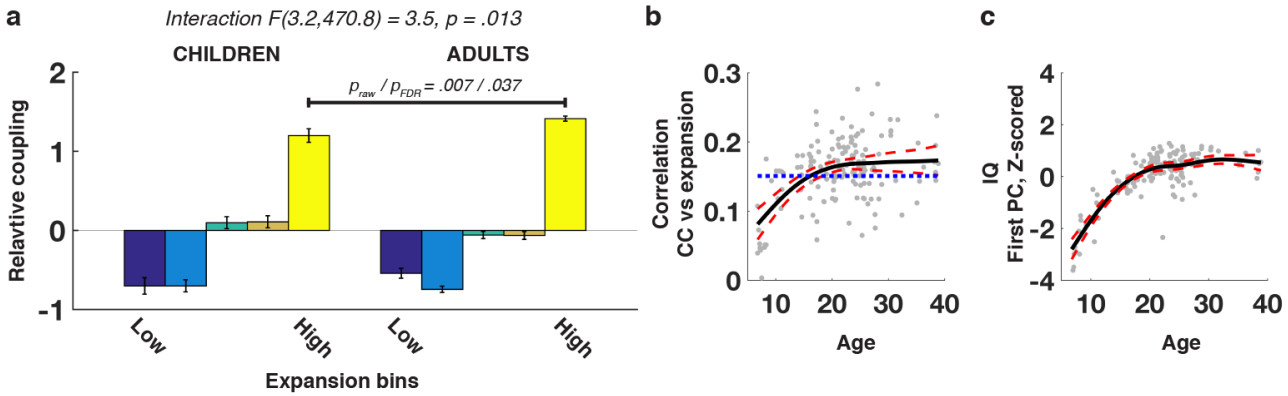

914

915 *Figure 3*

916

Supplementary Material

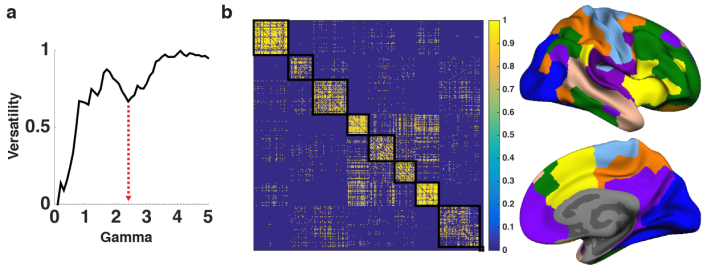

Spearman correlations with node expansion

Edge density (%)	Optimal gamma	Graph measures: Participation coefficient	Betweenness centrality	Within-module degree	Strength
5	2.2	**0.28**	**0.22**	0.06	-0.09
6	2.3	**0.38**	**0.28**	0.07	-0.06
7	2.1	**0.41**	**0.32**	0.09	-0.03
8	2.1	**0.53**	**0.33**	0.11	-0.02
9	2.4	**0.54**	**0.32**	0.16	-0.02
10	2.4	**0.54**	**0.33**	0.15	0.00
15	1.5	**0.32**	**0.30**	0.15	0.06
20	1.5	**0.23**	**0.25**	0.16	0.09
Average		**0.51**	**0.29**	0.14	0.00

Supplementary Figure 1. (a) Versatility (Shinn et al. 2017) was calculated over several resolution parameters for each thresholded graph (gamma 0.1-5.0 in steps of 0.1). Shown is mean versatility per value of gamma estimated over 500 iterations. The gamma minimizing mean versatility was used as the resolution parameter for modular decomposition of the thresholded graph, with the additional criterion that the resulting decomposition consisted of more than 3-4 modules. This last criterion implies a tradeoff weighting network resolution over decomposition stability, and was included to promote solutions with similar number of modules to what is commonly reported in the literature (Yeo et al. 2011; Power et al. 2013; Bertolero et al. 2015). In the present example (graph thresholded at 10% edge density), gammas below 1.2 were associated with low versatility (i.e. high stability in estimating communities), however at this resolution level only 3 modules were produced. The next "dip" was found at gamma=2.4, which resulted in a local stable solution consisting of 9 modules. (b) Connectivity matrix thresholded at 10% edge density. Black outlines show the communities resulting from the modular decomposition - shown in different colors on the cortical surface to the right. (c) Spearman correlations between estimated network measures and evolutionary expansion per node at different edge density thresholds. Bold numbers indicate a significant corrected correlation ($p<.05/4$).

			Graph measures			
		Optimal gamma	Participation coefficient	Betweenness centrality	Within-module degree	Strength
Edge density (%)	*5*	1.5	**0.26**	**0.30**	0.07	**0.28**
	6	1.5	**0.31**	**0.33**	0.13	**0.28**
	7	1.4	**0.37**	**0.35**	**0.21**	**0.28**
	8	1.5	**0.22**	**0.31**	**0.22**	**0.27**
	9	1.4	**0.31**	**0.32**	**0.20**	**0.26**
	10	1.4	**0.25**	**0.28**	0.19	**0.25**
	15	0.9	**0.29**	**0.28**	0.16	**0.22**
	20	1.1	**0.23**	**0.26**	0.15	**0.19**
	Average		**0.41**	**0.27**	0.17	**0.25**

Supplementary Figure 2. Spearman correlations between estimated network measures and evolutionary expansion calculated on functional connectivity data after weighting by Euclidean distance between nodes. Bold numbers indicate a significant corrected correlation ($p < .05/4$).

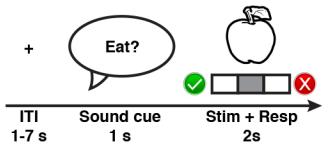

Supplementary Figure 3. Following a jittered intertrial-interval, an fMRI trial consisted of a voice asking a question ("Can you eat it?" or "Can you lift it?") and the presentation of a drawn object. The participant's task was to indicate with a button press whether the action-item association could be performed or not. See (Sneve et al. 2015) for additional details about the paradigm.

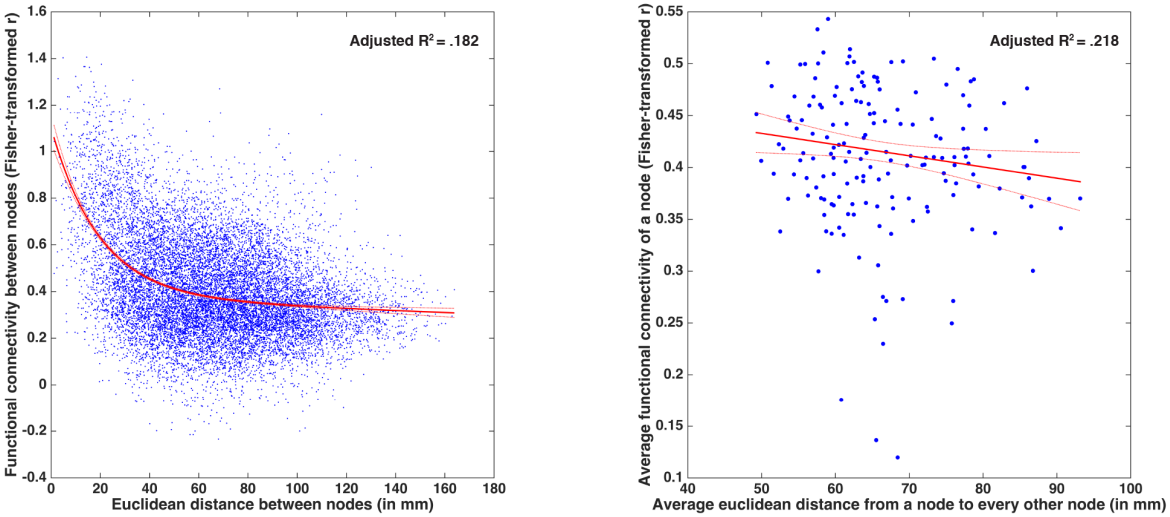

946

947 *Supplementary Figure 4.* Left panel: plot showing average functional connectivity across participants between two right-
948 hemispheric nodes from the custom cortical parcellation, as a function of Euclidean distance between the two nodes.
949 Overlaid is a two-term exponential fit, maximizing adjusted R^2. Edges characterized by short physical distance tend to show
950 higher connectivity than edges representing nodes far apart in physical space. Right panel: plot showing average functional
951 connectivity of a node (mean connectivity across every edge containing a node) as a function of the average physical
952 distance from that node to all other nodes in the right hemisphere. Overlaid is a robust single-term polynomial fit
953 demonstrating that for nodes with mean global connectivity > ≈.30, more centrally placed nodes (in physical space) tend to
954 have stronger global connectivity.

955

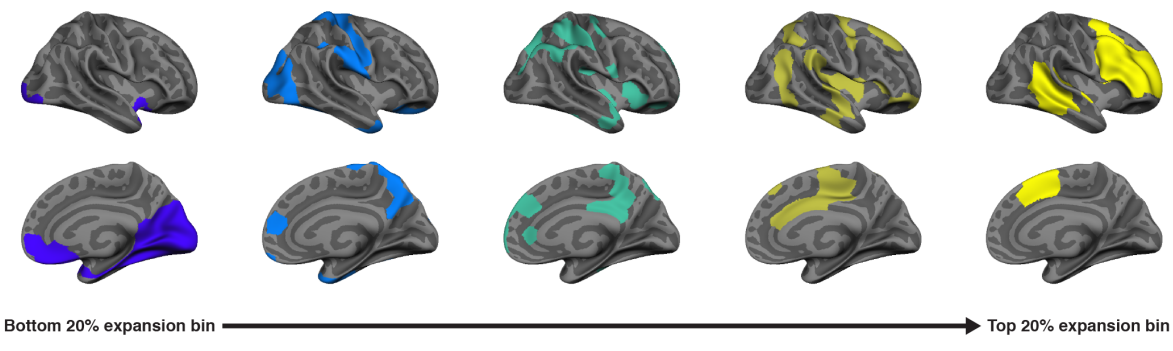

Supplementary Figure 5. Expansion bins in 20% steps ("Hotspots" in bright yellow to the right)

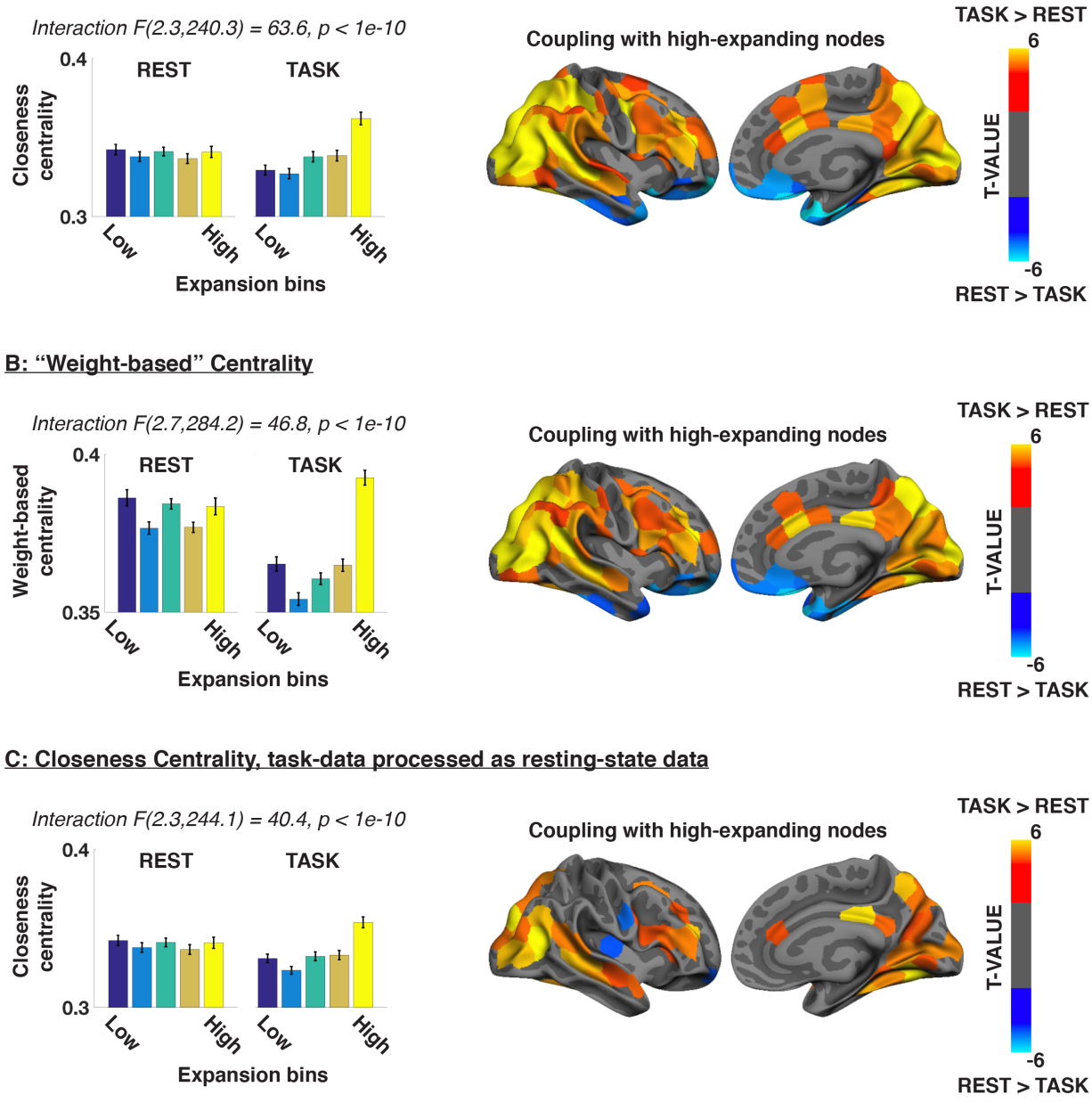

Supplementary Figure 6. Control analyses on data weighted by the Euclidean distance between nodes. (A) shows the same data as presented in Fig. 2, to facilitate comparisons with the results from control analyses. (B) shows the state-dependent coupling analyses performed on functional connectivity (edge) weights directly, i.e. avoiding the step of mapping weights to path lenghts. (C) shows the state-dependent coupling analyses performed following similar pre-processing and analysis of the data from the two states (i.e., analyzing task data following the resting-state analysis pipeline as described in the manuscript, rather than using correlational PPI). Note that, as in the main analyses, edge-wise connectivity weights were normalized by the average weight in the matrix before calculating centrality measures in the control analyses, to allow for comparisons of weighted graph measures from different states (Opsahl et al., 2010).

A: Original analyses (as in Fig. 2) – not weighted by Euclidean distance

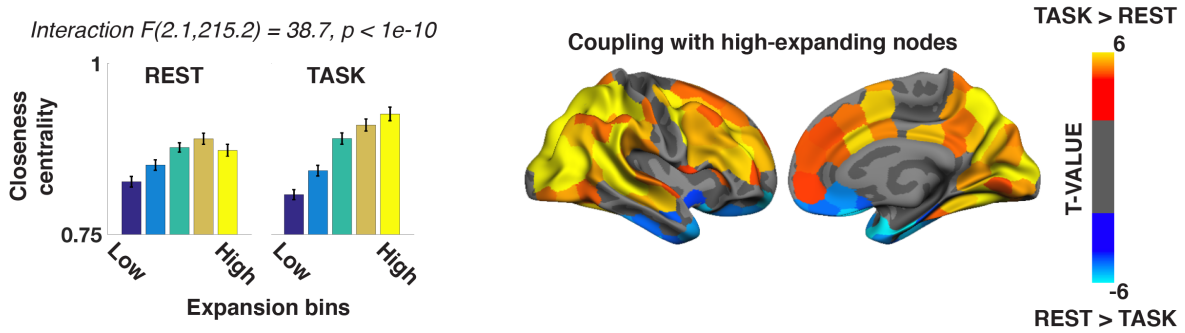

B: "Weight-based" Centrality – not weighted by Euclidean distance

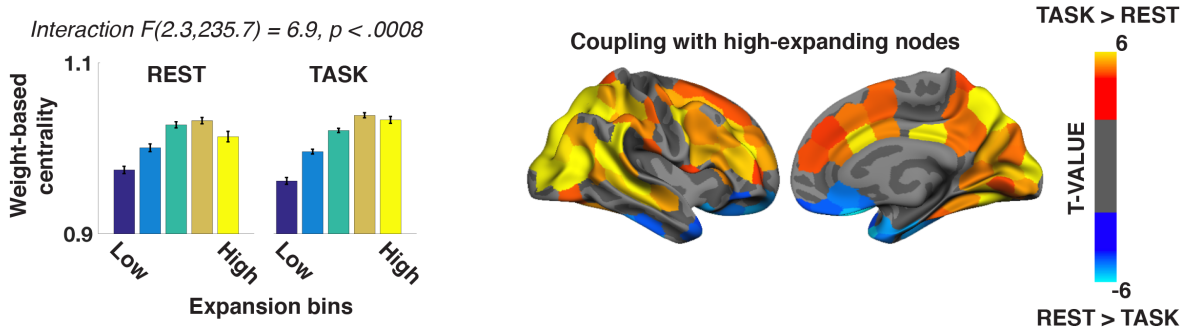

C: Closeness Centrality, task-data processed as resting-state data – not weighted by Euclidean distance

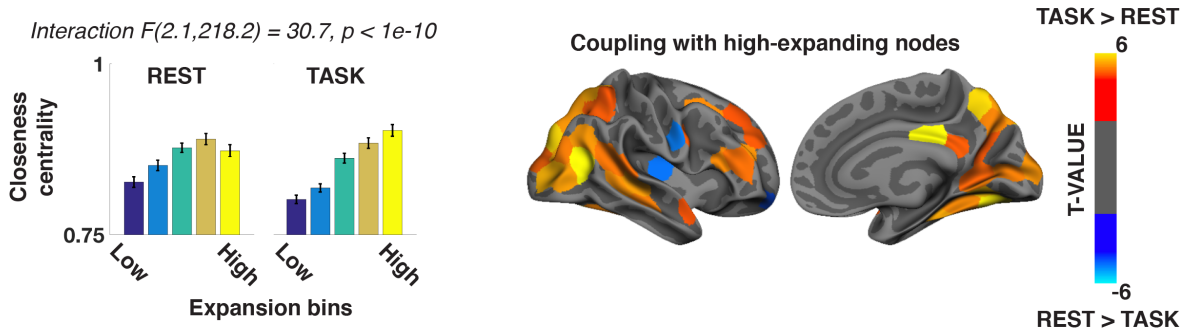

Supplementary Figure 7. Control analyses on data *not* weighted by the Euclidean distance between nodes. All analyses were performed as described in manuscript Fig. 2 and SFig. 6.

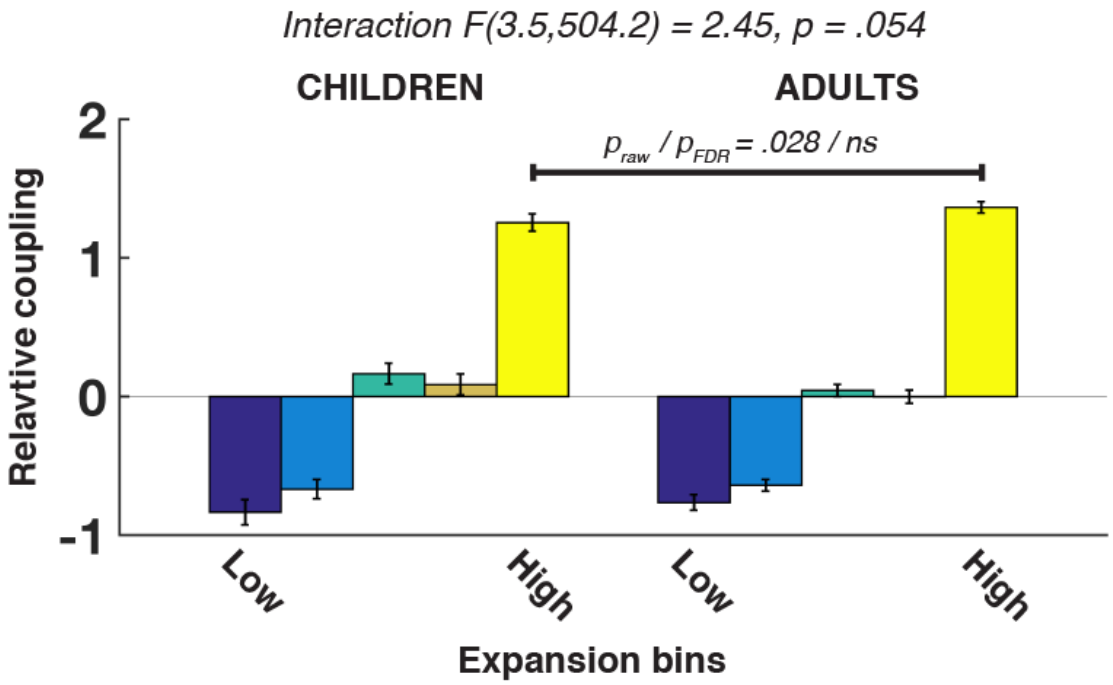

Supplementary Figure 8. Comparison of evolutionary high-expanding cortex' functional coupling across age groups, after regression of motion measures from the data. Analyses were otherwise performed as described in manuscript Fig. 3. Note that to calculate FDR-corrected p-values, at least one of the tested p-values has to pass the "Bonferroni-criterion" (in the current context, .05/5). We therefore only report uncorrected p-values for the post-hoc test comparing relative coupling between children and adults' high-expanding nodes.

Supplementary References

Bertolero MA, Yeo BTT, D'Esposito M. 2015. The modular and integrative functional architecture of the human brain. Proc Natl Acad Sci U S A. 112:E6798-807.

Opsahl T, Agneessens F, Skvoretz J. 2010. Node centrality in weighted networks: Generalizing degree and shortest paths. Soc Networks. 32:245–251.

Power JD, Schlaggar BL, Lessov-Schlaggar CN, Petersen SE. 2013. Evidence for hubs in human functional brain networks. Neuron. 79:798–813.

Shinn M, Romero-Garcia R, Seidlitz J, Váša F, Vértes PE, Bullmore E. 2017. Versatility of nodal affiliation to communities. Sci Rep. 7:4273.

Sneve MH, Grydeland H, Nyberg L, Bowles B, Amlien IK, Langnes E, Walhovd KB, Fjell AM. 2015. Mechanisms Underlying Encoding of Short-Lived Versus Durable Episodic Memories. J Neurosci. 35:5202–5212.

Yeo BTT, Krienen FM, Sepulcre J, Sabuncu MR, Lashkari D, Hollinshead M, Roffman JL, Smoller JW, Zöllei L, Polimeni JR, Fischl B, Liu H, Buckner RL. 2011. The organization of the human cerebral cortex estimated by intrinsic functional connectivity. J Neurophysiol. 106:1125–1165.